JPE 17-5-21

https://doi.org/10.6113/JPE.2017.17.5.1338
ISSN(Print): 1598-2092 / ISSN(Online): 2093-4718

Modified RCC MPPT Method for Single-stage Single-phase Grid-connected PV Inverters

Chaiyant Boonmee* and Yuttana Kumsuwan†

*,†Department of Electrical Engineering, Faculty of Engineering, Chiang Mai University, Chiang Mai, Thailand

Abstract

In this study, a modified ripple correlation control (RCC) maximum-power point-tracking (MPPT) algorithm is proposed for a single-stage single-phase voltage source inverter (VSI) on a grid-connected photovoltaic system (GCPVS). Unlike classic RCC methods, the proposed algorithm does not require high-pass and low-pass filters or the increment of the AC component filter function in the voltage control loop. A simple arithmetic mean function is used to calculate the average value of the photovoltaic (PV) voltage, PV power, and PV voltage ripples for the MPPT of the RCC method. Furthermore, a high-accuracy and high-precision MPPT is achieved. The performance of the proposed algorithm for the single-stage single-phase VSI GCPVS is investigated through simulation and experimental results.

Key words: Arithmetic mean function, Grid-connected photovoltaic system, Maximum-power point tracking, Ripple correlation control, Single-stage single-phase voltage source inverter

I. INTRODUCTION

A grid-connected photovoltaic system (GCPVS) with single-stage single-phase voltage source inverter (VSI) is a direct power conversion from a photovoltaic (PV) array into the utility grid. GCPVS consists of a PV string, a decoupling capacitor, a half/full-bridge inverter located through the inductor, and a controller unit, which are shown in Fig. 1. This topology is a buck-type string inverter where the suitable DC bus voltage is mostly required at the least highest peak value of the utility grid voltage. It is favored for a few kilowatt ranges due to its benefits of high efficiency and reliability, small size, uncomplicated control method, and low cost [1]-[7]. With the controller unit, the maximum power point (MPP) of the PV string can be continuously achieved in every operating condition and in the power control.

The improved designs of the perturb and observe (P&O) methods, which were in accordance with the MPPT algorithms, were presented in [8]-[12]. All of these algorithms provide higher performance compared to the classical P&O method. A power measurement was proposed in [9] to precisely identify how much power change was produced from the change in irradiation, which is called the optimized dP-P&O method. This method can track the MPP accurately. In [10], the direction of varying irradiation can be estimated correctly. On the basis of this method, the power losses caused by rapidly changing irradiation can be significantly reduced. However, to accomplish the two solutions reported in [9] and [10], the controller still requires more time and higher performance. In [11], a wide-bandwidth DC voltage control loop of the P&O method was improved. However, this method cannot efficiently ensure the stability of the PV system at any operating condition. In [12], a proper design procedure for the sliding-mode controllers was compiled to ensure the stability of MPPT requirements, but this method needed the low-pass (LP) filter and was much more complex than the classical P&O method. The hill climbing and incremental conductance MPPT algorithms were reported in [13] and [14]. The performance of both MPPT methods depended on the sampling time and the step size of perturbation. By contrast, the ripple correlation control (RCC) MPPT algorithms were proposed in [15]-[20]. Compared with the method in [9]-[12] and [13], [14], the RCC MPPT method does not need the step perturbation to achieve the MPP due to the inherent gradient increment feature approach to the MPP, which can be simply implemented through an analog or digital circuit. The use of the RCC MPPT method for a DC–DC converter, which

Manuscript received Apr. 11, 2017; accepted Jun. 23, 2017
Recommended for publication by Associate Editor Jong-Bok Baek.
†Corresponding Author: yt@eng.cmu.ac.th
Tel: +66-5394-4135 to 4140, Fax: +66-5394-4195, Chiang Mai Univ.
*Dept. of Electrical Eng., Faculty of Eng., Chiang Mai Univ., Thailand

proved the high performance of this algorithm, was reported in [15] and [16]. An extreme seeking method for the RCC MPPT method used for a grid-connected inverter was proposed in [17]. Based on this method, the HP filter is still used to obtain the desired ripples. In [18], the modified extreme seeking control for a boost DC–DC converter was also reported. In [19], a combination of the RCC MPPT method and the model reference adaptive control method was addressed to eliminate the overshoot produced by using the conventional MPPT algorithm. In addition, an RCC MPPT method for the single-stage single-phase GCPVS was introduced in [20]. This method requires the first-order HP and LP filters to generate the ripples of the PV power, PV voltage, and desired average value of the ripple product. However, some of the drawbacks to these ripples and this average value depend on their time constants and the need to eliminate the AC component, which is included in the measured PV voltage, for a PI voltage controller. Most of these drawbacks are results of the reduction in the performance of tracking and the efficiency of the PV system.

To solve these drawbacks, the utilization of the moving average filter, which is sometimes called arithmetic mean function, is used in many applications [21] and was firstly applied into the MPPT algorithm for the single-stage single-phase VSI GCPVS in [22] and [23]. This development modifies the conventional RCC MPPT method, which then enabled the method to simply and precisely extract the valid AC and DC components required in the MPPT method without the carefulness of the time constant designs in HP and LP filters and the increment of the AC component filter function in the PI DC voltage controller. In this study, the modified RCC MPPT method for the single-stage single-phase VSI GCPVS is extended with deep analysis and comprehensive study on the accounts of the arithmetic mean function principle along with its modification in the proposed MPPT method, the selection of the suitable integral gain for an integrator in the proposed MPPT method, and the details of the cascade loop controllers for the single-stage single-phase VSI GCPVS. Moreover, the modified RCC MPPT method is challenged by the simulation results directly compared with the experimental results, which can confirm the feasibility of the proposed control scheme for the single-stage single-phase VSI GCPVS and can also be compared with the existing and well-known RCC MPPT and P&O MPPT methods.

II. CONVENTIONAL RCC MPPT METHOD

The zero partial derivative of the PV power to the PV voltage $\partial p_{\mathrm{PV}} / \partial v_{\mathrm{PV}} = 0$ is the essential value used to verify the MPP of the PV system. Furthermore, the change in PV power ∂p_{PV} and the PV voltage ∂v_{PV} act as the AC components or the ripples of the PV power $\tilde{p}_{\mathrm{PV}}$ and the PV voltage $\tilde{v}_{\mathrm{PV}}$,

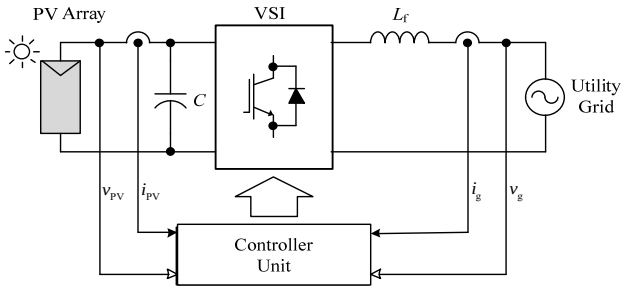

Fig. 1. The power scheme of the single-stage single-phase VSI GCPVS.

respectively, which can be described as follows [20]:

$$\frac{\tilde{p}_{\mathrm{PV}}}{\tilde{v}_{\mathrm{PV}}} \cong \frac{\partial p_{\mathrm{PV}}}{\partial v_{\mathrm{PV}}} \cong 0 . \tag{1}$$

In [8]–[12], the MPP of the PV systems is achieved by adapting the function of the derivative of power to voltage in terms of ripples in Eq. (1) to avoid the critical calculation of the instantaneous power and voltage ripples by averaging the product of these ripples with the PV voltage ripple $\tilde{v}_{\mathrm{PV}}$, which is given by

$$\frac{\partial p_{\mathrm{PV}}}{\partial v_{\mathrm{PV}}} \cong \frac{\dfrac{1}{T_{\mathrm{rip}}}\displaystyle\int_{t-T}^{t}\left(\tilde{p}_{\mathrm{PV}}\tilde{v}_{\mathrm{PV}}\right)dt}{\dfrac{1}{T_{\mathrm{rip}}}\displaystyle\int_{t-T}^{t}\tilde{v}_{\mathrm{PV}}^{2}dt} \cong \frac{\overline{\tilde{p}_{\mathrm{PV}}\tilde{v}_{\mathrm{PV}}}}{\overline{\tilde{v}_{\mathrm{PV}}\tilde{v}_{\mathrm{PV}}}}, \tag{2}$$

where T_{rip} is a cycle time of ripples. On the basis of (2), the sign of the derivative of power to voltage can be adapted directly along the average of the product $\overline{\tilde{p}_{\mathrm{PV}}\tilde{v}_{\mathrm{PV}}}$ due to the average of $\tilde{v}_{\mathrm{PV}}^{2}$, which is always a positive value. Therefore, this sign value is adequate to track the MPP PV voltage as follows:

$$\operatorname{sign}\left(\frac{\partial p_{\mathrm{PV}}}{\partial v_{\mathrm{PV}}}\right) \cong \operatorname{sign}\left(\overline{\tilde{p}_{\mathrm{PV}}\tilde{v}_{\mathrm{PV}}}\right) \begin{cases} = +1 & if \quad v_{\mathrm{MPP}} > v_{\mathrm{PV}} \\ = 0 & if \quad v_{\mathrm{MPP}} = v_{\mathrm{PV}} \\ = -1 & if \quad v_{\mathrm{MPP}} < v_{\mathrm{PV}} \end{cases} . \tag{3}$$

Three situations of the sign signal are $+1$, 0, and -1, and they are used to indicate an increase, standby, and decrease in the PV voltage v_{PV} for tracking the MPP PV voltage v_{MPP}, respectively. To achieve the sign as (3), the power and voltage ripples have to be obtained correctly as the basic theory of the AC components or ripples, which is calculated by

$$\tilde{p}_{\mathrm{PV}} = p_{\mathrm{PV}} - \overline{p}_{\mathrm{PV}} \text{ and } \tilde{v}_{\mathrm{PV}} = v_{\mathrm{PV}} - \overline{v}_{\mathrm{PV}}, \tag{4}$$

where $\overline{p}_{\mathrm{PV}}$ and $\overline{v}_{\mathrm{PV}}$ are the average PV power and PV voltage, respectively. Furthermore, a method that obtains the desired ripples exploited by the conventional RCC MPPTs [15]-[20] is used in the HP filter to avoid the DC component and let the LP filters average the product of ripples $\overline{\tilde{p}_{\mathrm{PV}}\tilde{v}_{\mathrm{PV}}}$. Although the use of the filters is not complex and achieving the desired ripples or average with only one process is easy, it still has some drawbacks with respect to the definitions of the suitable time constants for the HP and LP filters to produce a

high level of accuracy of the sign signal, which is still required as a period of time to expand the time delay for indicating the MPP of the sign signal. As mentioned, to improve the method that aims to harvest the high-performance MPP indicator with the desired sign signal, the modified RCC MPPT method is then proposed using the arithmetic mean function algorithm, which is discussed in Section III.

III. Proposed Modified RCC MPPT Method

Using the proposed modified RCC MPPT method, which is directly based on the operation of the sign signal, it is dependent on the average product between the ripples of PV power $\tilde{p}_{PV}$ and PV voltage $\tilde{v}_{PV}$, which are used for tracking the MPP. With this method, the conventional method discussed in Section II is modified by applying the arithmetic mean function principle, as further discussed in Section III-A, instead of the HP and LP filters to extract the AC components, which are the ripples of PV power $\tilde{p}_{PV}$ and PV voltage $\tilde{v}_{PV}$, and the DC components, which is the average product of $\overline{\tilde{p}_{PV}\tilde{v}_{PV}}$, respectively, as analyzed in Section III-B. Subsequently, the relative selection of the suitable integral gain K_{dv} in the proposed MPPT algorithm is accordingly considered in Section III-C. Additionally, the cascade loop control represented by the DC voltage controller and the grid-connected current controller is addressed in Section III-D.

A. Principle of Arithmetic Mean Function

The typical principle of the arithmetic mean function (MF) in continuous-time domain [21], with the arbitrary input signal $x(t)$, can be defined as

$$\overline{x}(t)=\frac{1}{T_w}\int_{t-T_w}^{t}x(t)dt, \tag{5}$$

where T_w is the time window width used to calculate the arithmetic mean function of the input signal $x(t)$. To determine its behavior in the frequency domain, by taking the Laplace transform into (5), the transfer function of the arithmetic mean function can be expressed as

$$\mathrm{MF_{DC}}(s)=\frac{\overline{X}(s)}{X(s)}=\frac{1-e^{-T_w s}}{T_w s}. \tag{6}$$

Replacing $s=j\omega$ in (6), the arithmetic mean function characteristics through the bode plot for giving $T_w=0.01$ s with consideration of low frequency (1 Hz) to high frequency (1 kHz) is represented in Fig. 2(a). In this figure, the arithmetic mean function can block the AC component of the input signal $x(t)$ for all the integer multiples of frequency $1/T_w$. This finding means that it can easily extract the DC component in the input signal $x(t)$, which has the fundamental frequency $f_w=1/T_w$, with good odd and/or even harmonic elimination.

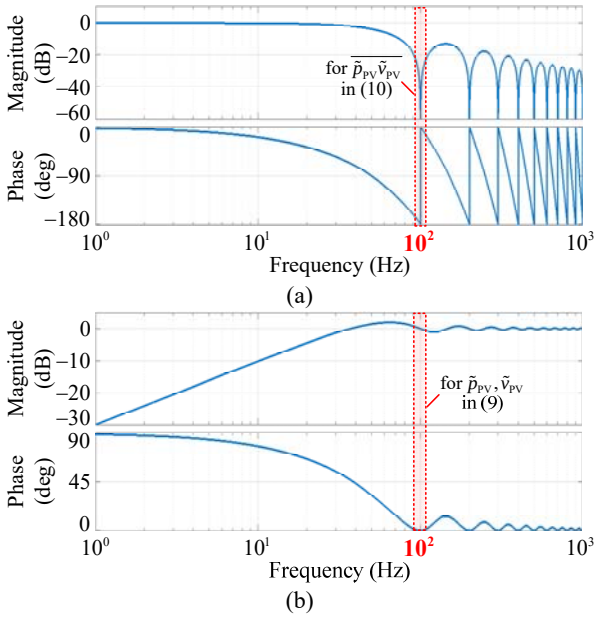

Fig. 2. Bode plots of arithmetic mean function principle for $f_w=1/T_w=100$ Hz : (a) DC component extraction, (b) AC component extraction.

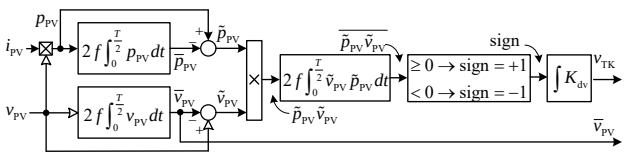

Fig. 3. Block diagram of proposed modified RCC MPPT method.

The pure AC component of the arbitrary input signal $x(t)$ can be achieved by modifying the operation of the arithmetic mean function as follows:

$$\tilde{x}(t)=x(t)-\overline{x}(t)=x(t)-\frac{1}{T_w}\int_{t-T_w}^{t}x(t)dt\,. \tag{7}$$

Likewise, its frequency appearance can be checked by taking the Laplace transforms in (7). Thus, the transfer function is

$$\mathrm{MF_{AC}}(s)=\frac{\tilde{X}(s)}{X(s)}=\frac{e^{-T_w s}+T_w s-1}{T_w s}=1-\mathrm{MF_{DC}}(s)\,. \tag{8}$$

The bode plot of (8) is shown in Fig. 2(b) with the capability of pure AC component extraction in the input signal $x(t)$, which means that it can provide the desired peak value without shifting the phase of the AC component for the case of the fundamental frequency of the input signal $x(t)$ being $f_w=1/T_w$.

B. Modified RCC MPPT Method

As shown in Fig. 3, the key idea of the proposed modified RCC MPPT method is using the arithmetic mean function, which is a much simpler theoretical principle with high precision of DC and AC component extractions regardless of

the complicated design of the relevant parameters in time constants compared to other filters. First, to achieve the ripples of PV power $\tilde{p}_{PV}$ and PV voltage $\tilde{v}_{PV}$ from the measured instantaneous PV power p_{PV} and PV voltage v_{PV}, respectively, these ripples can be obtained using the concept of (7), resulting in

$$\tilde{p}_{PV} = p_{PV} - 2f\int_0^{\frac{T}{2}} p_{PV}dt \text{ and } \tilde{v}_{PV} = v_{PV} - 2f\int_0^{\frac{T}{2}} v_{PV}dt . \quad (9)$$

In (9), due to the proposed MPPT method applied in the single-stage single-phase VSI GCPVS, the grid frequency is $f = 50$ Hz and $T = 1/f$ is a time period of the grid. Thus, the frequencies of the ripples of PV power $\tilde{p}_{PV}$ and PV voltage $\tilde{v}_{PV}$ are twice the grid frequency (100 Hz). Therefore, the time window widths used to calculate the ripples of PV power $\tilde{p}_{PV}$ and PV voltage $\tilde{v}_{PV}$ are set at $T_w = 1/2f = 0.01$ s, which produces pure ripples of the PV power $\tilde{p}_{PV}$ and PV voltage $\tilde{v}_{PV}$ with the desired peak values of the ripples and the constant 100 Hz frequency, as exemplified in the shaded area of Fig. 2(b).

After achieving the ripples of the PV power $\tilde{p}_{PV}$ and PV voltage $\tilde{v}_{PV}$ of Eq. (9), the product of the ripples $\tilde{p}_{PV}\tilde{v}_{PV}$ is then activated and its frequency still resembles the ripples of the PV power $\tilde{p}_{PV}$ and PV voltage $\tilde{v}_{PV}$. Consequently, the average of product $\overline{\tilde{p}_{PV}\tilde{v}_{PV}}$ can be forwarded into the processing of the sign signal computation by considering the concept of (5) as

$$\overline{\tilde{p}_{PV}\tilde{v}_{PV}} = 2f\int_0^{\frac{T}{2}} \tilde{p}_{PV}\cdot\tilde{v}_{PV}dt . \quad (10)$$

From Eq. (10), it is also achieved using the same time window widths T_w as (9), which is why the DC component can be surely decomposed by blocking the 100 Hz product ripple $\tilde{p}_{PV}\tilde{v}_{PV}$ component, as illustrated in the shaded area of Fig. 2(a), as well as the other integer harmonic components in the product ripple $\tilde{p}_{PV}\tilde{v}_{PV}$. In addition, the average PV voltage $\overline{v}_{PV}$ is obtained by the same algorithm of (10), which further uses the design of the DC voltage controller (see Section III-D).

Then, the computation of the sign signal is conducted in the same way as (3) by using the comparative condition between the average product $\overline{\tilde{p}_{PV}\tilde{v}_{PV}}$ obtained from (10) and the reference zero to build the sign signal for tracking the MPP with a high precision and convenient mathematical implementation based on the account of the typical principle of the arithmetic mean function. However, the performance of the proposed MPPT method is also dependent on the defined value of the integral gain K_{dv}. The selection principle of the suitable integral gain K_{dv} for the system is

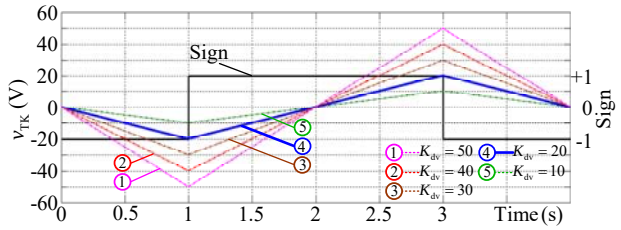

Fig. 4. Criteria for selecting the integral gain K_{dv}.

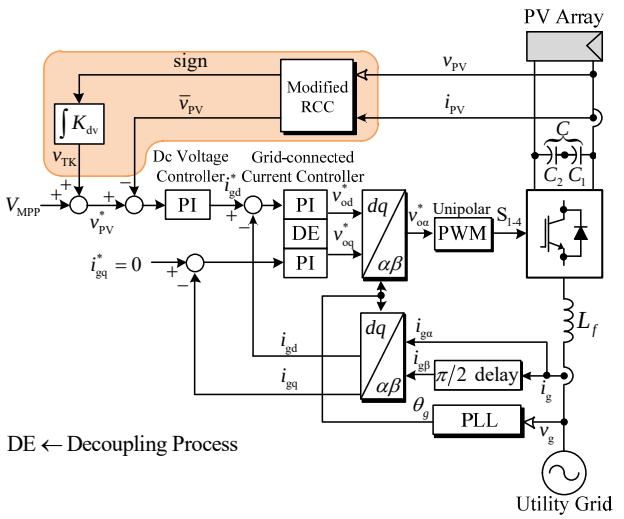

Fig. 5. Power and control scheme of proposed MPPT algorithm for single-stage single-phase VSI GCPVS.

explained in the following.

C. Selection Principle of Integral Gain K_{dv}

To generate a voltage waveform for detecting the tracking of the sign signal, an integrator, which produces a linear characteristic for the output with the speed depending on the slope offered by the integral gain K_{dv}, is transformed as

$$v_{TK} = \text{sign}\left(\overline{\tilde{p}_{PV}\tilde{v}_{PV}}\right)\cdot\left(\int K_{dv}dt\right), \quad (11)$$

where v_{TK} is the tracking voltage, which is a relative ramp output varying in accordance with the tracking of the input sign signal and K_{dv} is the integral gain of an integrator.

To reasonably select the suitable integral gain K_{dv} (see Eq. (11)) and achieve a good performance of the proposed MPPT algorithm for the single-stage single-phase VSI GCPVS, the simulated examples of the tracking voltages v_{TK} with five different integral gains K_{dv} of 50, 40, 30, 20, and 10 are illustrated, as shown in Fig. 4, in a case study of upward (-1→0→+1) and downward (+1→0→-1) transitions of the sign signal. The sign signal attempts to track the MPP with the sampling time of 2 s for a visible description. In the figure, the sign signal is initially −1, which leads to the continuous ramp down of each tracking voltage v_{TK} (see lines ①, ②, ③, ④, and ⑤) from $t = 0$ s with their slopes corresponding to the integral gains K_{dv}. When the sign signal can meet the MPP at $t = 1$ s, it is immediately

changed to +1 and the tracking voltages v_{TK} are also changed as ramp-up responses. The tracking voltages v_{TK} with the high integral gain $K_{dv} = 50$ can reach the MPP faster than those of the other gains. However, it also behaves as a large ripple, which is generally undesirable in PI controllers. By contrast, the tracking voltages v_{TK} may be too slow and unable to capture the MPP with low integral gain at $K_{dv} = 10$. Therefore, the use of the integral gain $K_{dv} = 20$ is effective enough for the proposed MPPT method, which means that it is fast enough to track the MPP with the agreeable compromise of the ripple magnitude of the tracking voltages v_{TK}, which is further transferred to a part of the cascade loop controllers, as shown in Fig. 5.

D. Cascade Loop Controllers

In the DC voltage controller, the PV voltage reference v_{PV}^* is generated by summing the rated MPP voltage V_{MPP} and the tracking voltage v_{TK} given by (11) to control the PV voltage v_{PV} that always operates on the MPP voltage V_{MPP}. Here, it can be expressed as

$$v_{PV}^* = V_{MPP} + v_{TK}, \tag{12}$$

where V_{MPP} is the initial value around the rated MPP voltage at the standard test condition (STC) of the PV array. To regulate the PV voltage v_{PV} following the MPP voltage of the PV array drawn by the reference PV voltage v_{PV}^*, a PI DC voltage controller is used to eliminate the steady-state error and achieve the MPP voltage, which is based on Kirchhoff's current law at the connected point among the PV array, the capacitor, and the inverter input terminals (see Fig. 5) as given by

$$i_C = i_{PV} - i_{INV} = C\frac{dv_C}{dt}, \tag{13}$$

where i_{INV} is the instantaneous input current of the inverter. Generally, the inverter and inductor filter (L_f) of the system are limited and have been omitted. Moreover, the PV power p_{PV} is the sum of the instantaneous capacitor power p_C and the instantaneous grid power p_g, which is equal to the instantaneous input power of inverter p_{INV}. The reference grid power can be calculated as

$$p_g^* = p_{INV}^* = v_{PV}(i_{PV} - C\frac{dv_C}{dt}). \tag{14}$$

From (14), to avoid some ripples included in the reference grid power p_g^*, the average PV voltage $\overline{v}_{PV}$ can be replaced with the instantaneous PV voltage v_{PV}, with the existing average PV voltage $\overline{v}_{PV}$, without extending the delay time.

In the grid-connected current controller, the main control objective for the proposed single-stage single-phase VSI GCPVS is to inject the active power into the grid with a unity power factor, which is based on the standard decoupling single-phase current control [7, 10]. From Eq. (3) and Fig. 3, if the average PV voltage $\overline{v}_{PV}$ is higher than the reference PV voltage v_{PV}^*, then the average PV voltage $\overline{v}_{PV}$ has to be reduced by increasing the grid current i_g, and then v_{PV}^* is negative and $\overline{v}_{PV}$ is positive. The value of the reference PV voltage v_{PV}^* is compared with the average PV voltage $\overline{v}_{PV}$ to generate an error signal. This signal is inputted into the PI voltage controller that determines the reference active power current component i_{gd}^*, whereas the reference reactive power current component i_{gq}^* is

$$i_{gd}^* = \frac{2p_g^*}{V_{gd}} \text{ and } i_{gq}^* = \frac{2q_g^*}{V_{gd}} = 0, \tag{15}$$

where q_g^* is the reactive power, V_{gd}, V_{gq} are the $d-q$ axis grid voltage components, $V_{gd} = |\hat{v}_g|$ is the peak value of the grid voltage $\hat{v}_g$, and the grid voltage of q axis is set to zero, $V_{gq} = 0$. From (15), the required reference inverter voltage and the PI current controllers with a decoupling process are used to regulate the reference inverter voltage components, v_{od}^* and v_{oq}^*, which are calculated by

$$\begin{bmatrix} v_{od}^* \\ v_{oq}^* \end{bmatrix} = L_f \frac{d}{dt}\begin{bmatrix} i_{gd}^* \\ i_{gq}^* \end{bmatrix} + \omega L_f \begin{bmatrix} -i_{gq}^* \\ i_{gd}^* \end{bmatrix} + \begin{bmatrix} V_{gd} \\ 0 \end{bmatrix}. \tag{16}$$

From the preceding equation, the variables are transformed to the $\alpha-\beta$ axis reference inverter voltage component $v_{o\alpha}^*$ by the position of the grid voltage (θ_g). A pulse width modulation (PWM) with unipolar technique is used to define the reference inverter voltage in the PWM block (see Fig. 5).

A simulation model in MATLAB/Simulink is built to investigate the performance of the considerable system working with the proposed MPPT method with a comparison between the selective integral gain $K_{dv} = 20$ and the other gains extending the discussion in Section III-C. Moreover, the relevant parameters in Section IV (see Table I) are carried out, as shown in Fig. 6. In the first condition, the irradiance G_i steps down from 1000 W/m^2 to 600 W/m^2 (see Fig. 6(a)). $K_{dv} = 20$ is selected, and the reference PV voltage v_{PV}^* in Fig. 6(b) and the reference active current i_{gd}^* in Fig. 6(c) are changed from the original MPP operation to the new MPP operation, where their speed MPP convergence is faster than that of the lower integral gain $K_{dv} = 10$. However, it is almost the same as those of the higher integral gains, but has a lower ripple, which is also more effective to transfer and operate PI controllers in DC-voltage loop control and grid-connected current loop control (see the zoomed period in Fig. 6(c)). The corresponding PV power p_{PV} can be

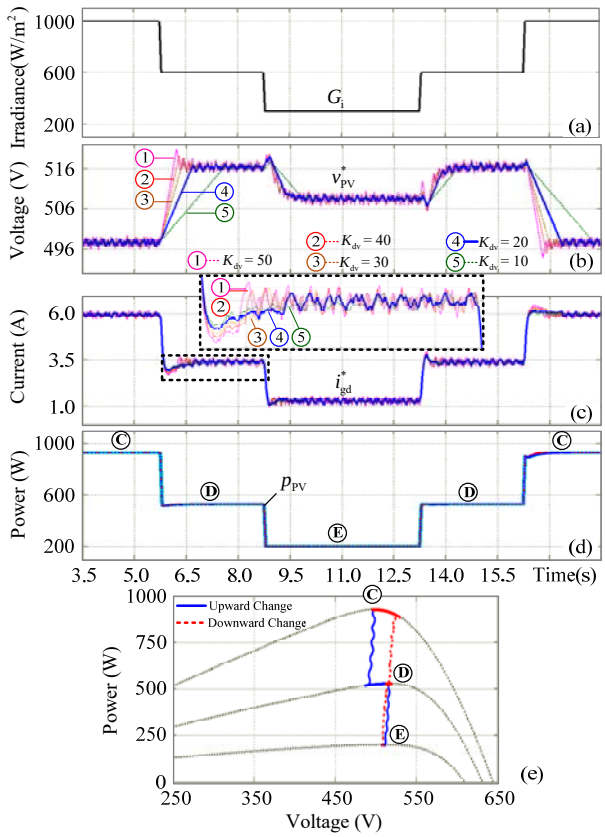

Fig. 6. Dynamics of power and control performances.

observed in Fig. 6(d), where the MPP PV power can be achieved and has a good step change from approximately 952 W to 556 W according to the step change of the irradiance G_i for all of the considerable integral gains, due to the agreeable work of the cascade loop controllers. This finding can also be examined by the corresponding *P–V* curve (Fig. 6(e)) from the MPP of period C to period D. Then, the next step-down change was from 600 $\mathrm{W/m^2}$ to 300 $\mathrm{W/m^2}$, and the returned-upward step changes also provided the same response, but only when operated at a different MPP, as shown from the transition of the MPP in period D to period E and the upward changes from period E to period D and further to period C.

IV. Simulation and Experimental Results

In this section, the proposed system presented as single-stage single-phase VSI GCPVS and the modified RCC MPPT method, as shown in Fig. 5, has been verified by the MATLAB/Simulink simulation environment, and the experimental implementation has been conducted on the laboratory prototype. Fig. 7 shows an overview diagram of the experimental prototype of the proposed system, which consists of two major parts. The first part is the controller using a dSPACE DS1104 controller via a CLP1104 input/output interface board commanded by a programmable

TABLE I
Main Designed Parameters of PV System

Parameters		Values
a-Si-based PV module (LSU58, Kaneka):		
Maximum power in STC	(P_{MPP})	58 Wp
Open-circuit voltage in STC	(V_{oc})	85 V
MPP voltage and current in STC	(V_{MPP}, I_{MPP})	63 V, 0.92 A
PV array:		
Rated power	(P_{rated})	928 W
Rated voltage and current	(V_{rated}, I_{rated})	504 V, 1.84 A
H-bridge VSI:		
Capacitors and inductor	(C_1, C_2)	2200 µF,8 mH
Switching frequency	(f_{sw})	14 kHz
PI controllers:		
Dc voltage controller	(K_{pv}, K_{iv})	0.08, 0.35
Grid-connected current controller	(K_{pc}, K_{ic})	15, 2000
Single-phase utility grid:		
Grid voltage and frequency	(V_g, f_l)	220 V, 50 Hz

computer (PC) system, where the sampling time rates of the cascade loop control are given by the DC voltage control and the grid-connected current control are set at 100 and 10 µs, respectively. The second part is the hardware included in the PV array source and the grid-connected VSI, which is controlled by the PWM signals with a deadtime of 4 µs. For a direct comparison, the parameters are set to be the same for the simulation and experiment, as shown in Table I. Significantly, the investigation considers the following points: i) to demonstrate the authentic precision of the proposed MPPT algorithm for the single-stage single-phase VSI GCPVS, ii) to demonstrate the dynamic performance of the proposed MPPT algorithm applied in the single-stage single-phase VSI GCPVS for interfacing with the single-phase utility grid, iii) and to evaluate the performance of the proposed system.

A. Precision of Modified RCC MPPT Method

Fig. 8 shows the close-up operation during the leading edge of the sign signal and the reliability of the proposed modified RCC MPPT method. This process is performed by commanding the PV current i_{PV} from 0 A to 1.25 A. Upon commencement (in area A), the PV power p_{PV} is lower than the MPP, which means that the MPP voltage is also lower than the PV voltage v_{PV}. Therefore, in this area, the average of the ripple product $\overline{\tilde{p}_{PV}\tilde{v}_{PV}}$ is maintained below 0, leading to "−1" for the sign signal. Consequently, the PV power p_{PV} and the PV current i_{PV} are continuously increased, except that the PV voltage v_{PV} is reduced. When the PV power p_{PV} is identical to the MPP, then the sign signal is precisely "0". The exact MPP occurs at the knee point of the PV power p_{PV}, and it can also corroborate the methodical precision of the proposed MPPT algorithm. Furthermore, the PV voltage

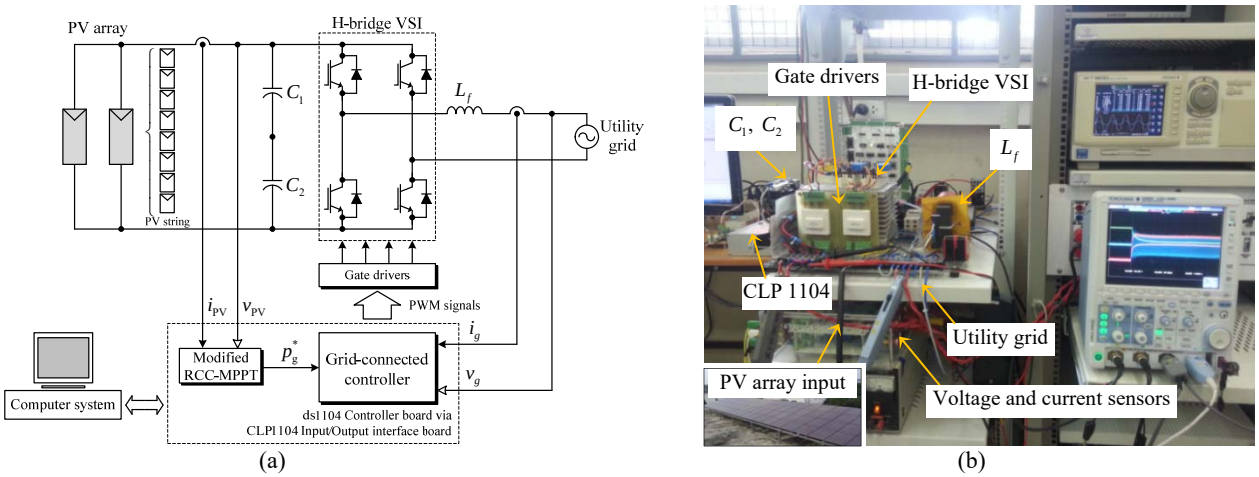

Fig. 7. Laboratory prototype setup of proposed system: (a) Diagram. (b) Photograph of hardware setup.

v_{PV} is lower than the MPP voltage and the sign signal is immediately changed to "+1," shown in area B. The PV current i_{PV} and the PV voltage v_{PV} still increase and decrease, respectively, and the PV power p_{PV} begins to reduce from the MPP accordingly. All those variables are constant during the last 2 s period on the rightmost side until the PV current i_{PV} is constrained as a constant of approximately 1.25 A. By contrast, the sign signal again changes from "+1" to "0" and "−1," respectively, when the PV voltage v_{PV} or the PV power p_{PV} are increased to the MPP. This finding means that the proposed MPPT method will always track the MPP to keep it constant. The good agreement between the simulation and experimental results can confirm the precision of the proposed MPPT method in theoretical modeling and real plant systems, as shown in Figs. 8(a) and (b), respectively.

B. Dynamic Performance of Modified RCC MPPT Method

The step response of the system based on the proposed modified RCC MPPT method is shown in Fig. 9. At period D, the PV power p_{PV} is initially at the MPP of approximately 36% of the rated power with a single string of the PV array. Then, it is changed to 72% of the rated power at period C by connecting the other remaining string to the PV array. Although the slight deviation of the PV voltage v_{PV} is drawn at the transient period, as observed in Fig. 9(a) (see the second trace), the system with the proposed MPPT method can immediately track the MPP. The system can also be inspected with the slight error position of the MPP voltage in the corresponding *P–V* curve at period D before changing the MPP of period C. The grid-connected active current i_{gd} accordingly provides a critical damped stepped-up response, whereas the reactive component can be commanded to keep the constant at zero, as shown in the third trace. Therefore, on the next trace, the unity power factor of the voltage and current for the grid side can be achieved in steady-state and dynamic operations. Subsequently, these aforementioned responses were conducted in the same way as the challenge of the stepped-down PV power from periods C to D. The experimental results are in good agreement with the corresponding behavior, as shown in Fig. 9(b). Sequentially, the instantaneous grid voltages v_g and currents i_g in the steady state of periods D and C are shown in Figs. 10(a) and 10(b) with a good unity power factor expression and THD_i qualities below 5% by 2.74% and 1.29%, respectively.

To demonstrate the sudden variation in the irradiance, the dynamic linear shading results of the simulation and experiment are shown in Figs. 11(a) and 11(b), respectively. The PV power p_{PV} and PV current i_{PV} are found to have a linear change with time $\Delta t = 0.3$ s. During the dynamic response, the grid current i_g is slightly affected and kept constant without the overshoot of a new MPP operation. Moreover, the *P–V* curves are shown with the corresponding operating points. The simulated and experimental results are also in good agreement, ensuring the validity of the MPPT approach.

Fig. 12 shows the comprehensive performance of the proposed modified RCC MPPT method (see Fig. 12(a)) because the beginning of the steady-state operation included the shading condition compared with the conventional RCC MPPT method (see Fig. 12(b)) and the P&O MPPT method (see Fig. 12(c)). The realistic solar irradiances in the real plant are $920\,W/m^2$, $882\,W/m^2$, and $910\,W/m^2$, respectively. With the proposed MPPT method in Fig. 12(a), the system is initially operated without the MPPT algorithm, and hereby the utility grid is fed by 0 W along with the absences of PV and grid currents, except that the PV voltage reaches approximately 600 V as it is the open-circuit voltage of the PV array. This operating period can be investigated at

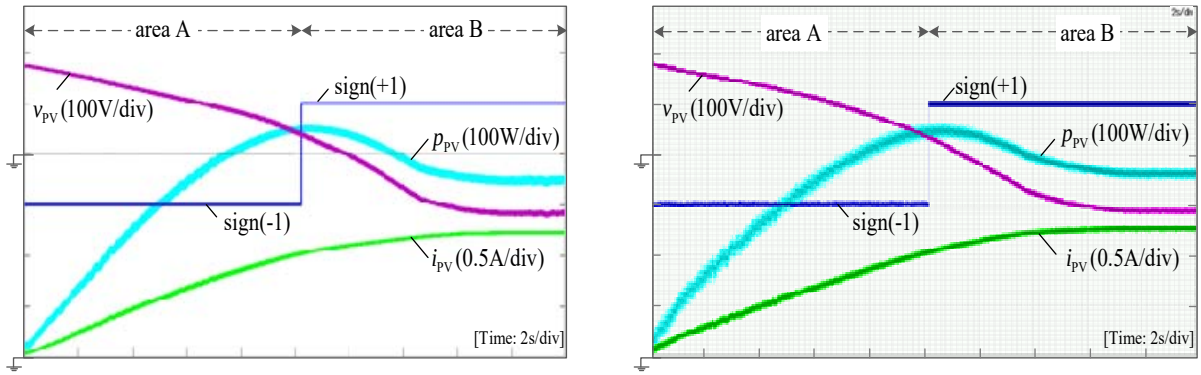

(a) (b)

Fig. 8. Verification in accuracy and precision of proposed modified RCC MPPT method by increasing PV current i_{PV} from 0 A to 1.25A. (a) Simulation results. (b) Experimental results.

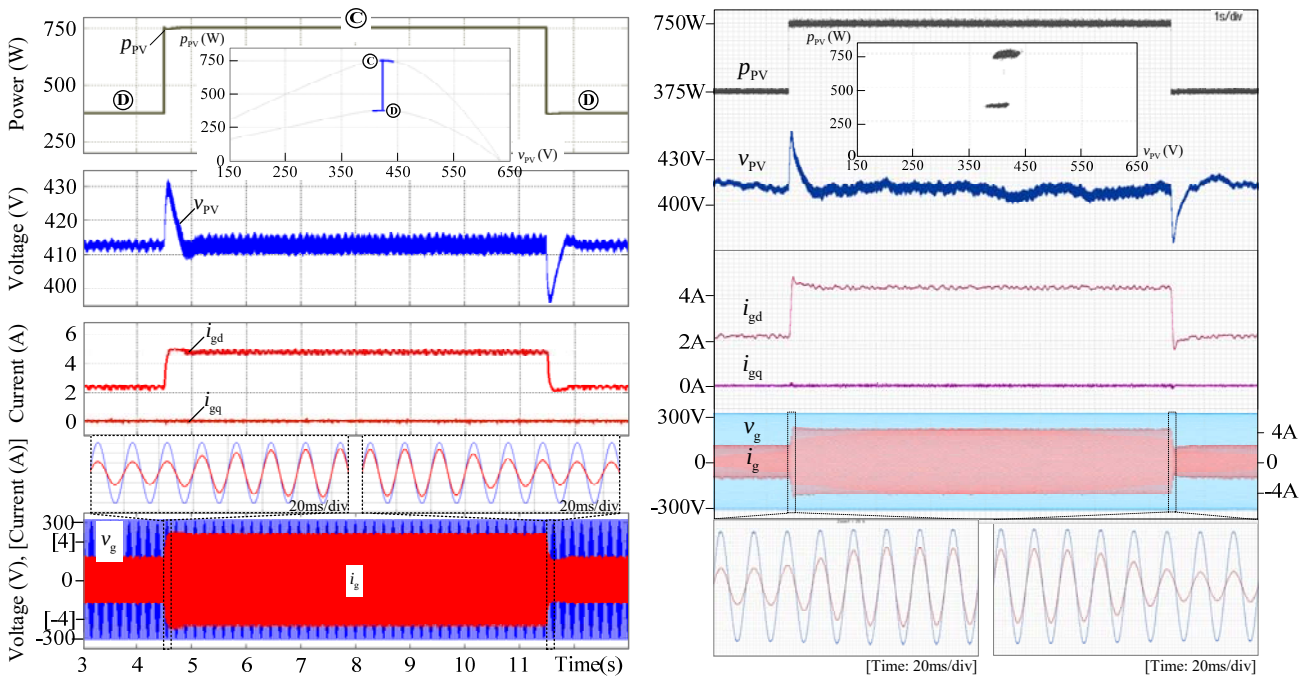

(a) (b)

Fig. 9. Dynamic response of system using proposed modified RCC MPPT method for step change of PV power. (a) Simulation results. (b) Experimental results.

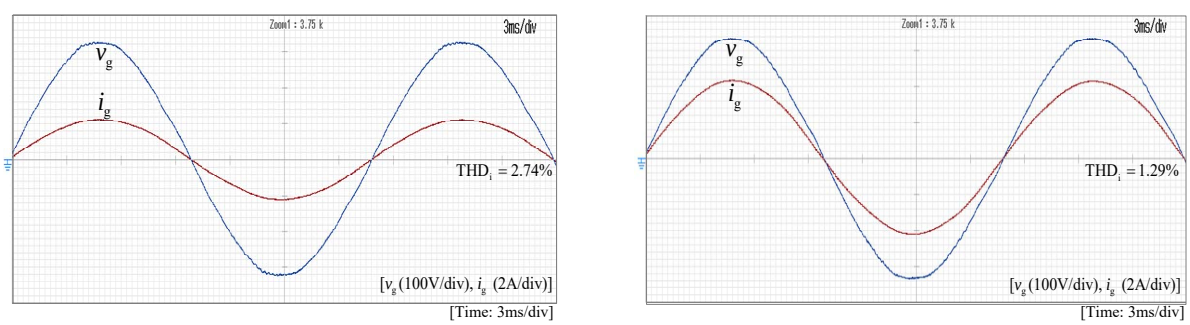

(a) (b)

Fig. 10. Steady-state experimental waveforms of the grid voltage v_g and current i_g reported in Fig. 9(b) with (a) PV power $p_{PV} = 375$ W and (b) the PV power $p_{PV} = 750$ W.

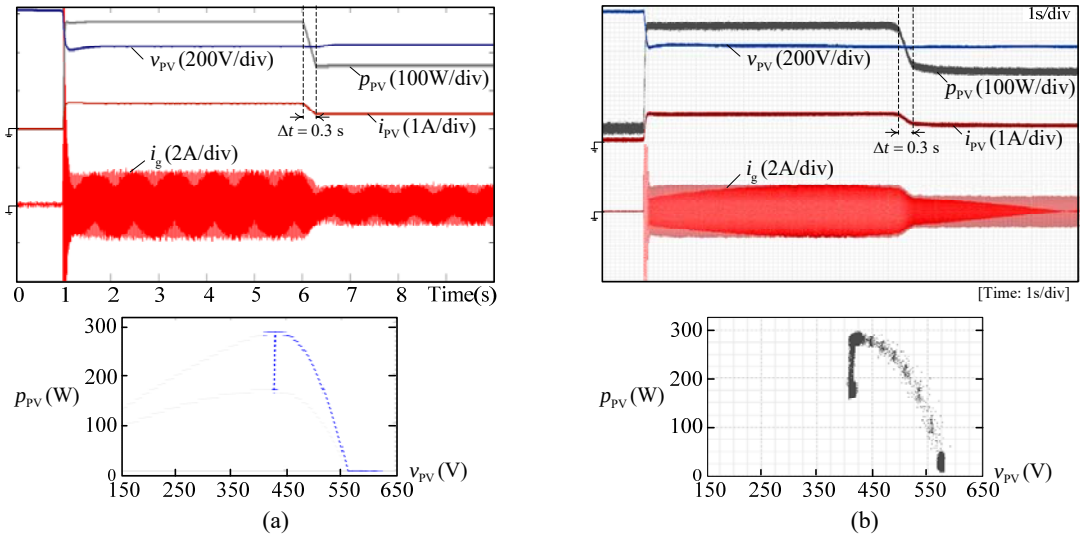

Fig. 11. Dynamic response of system using proposed modified RCC MPPT method for linear shading of PV power. (a) Simulation results. (b) Experimental results.

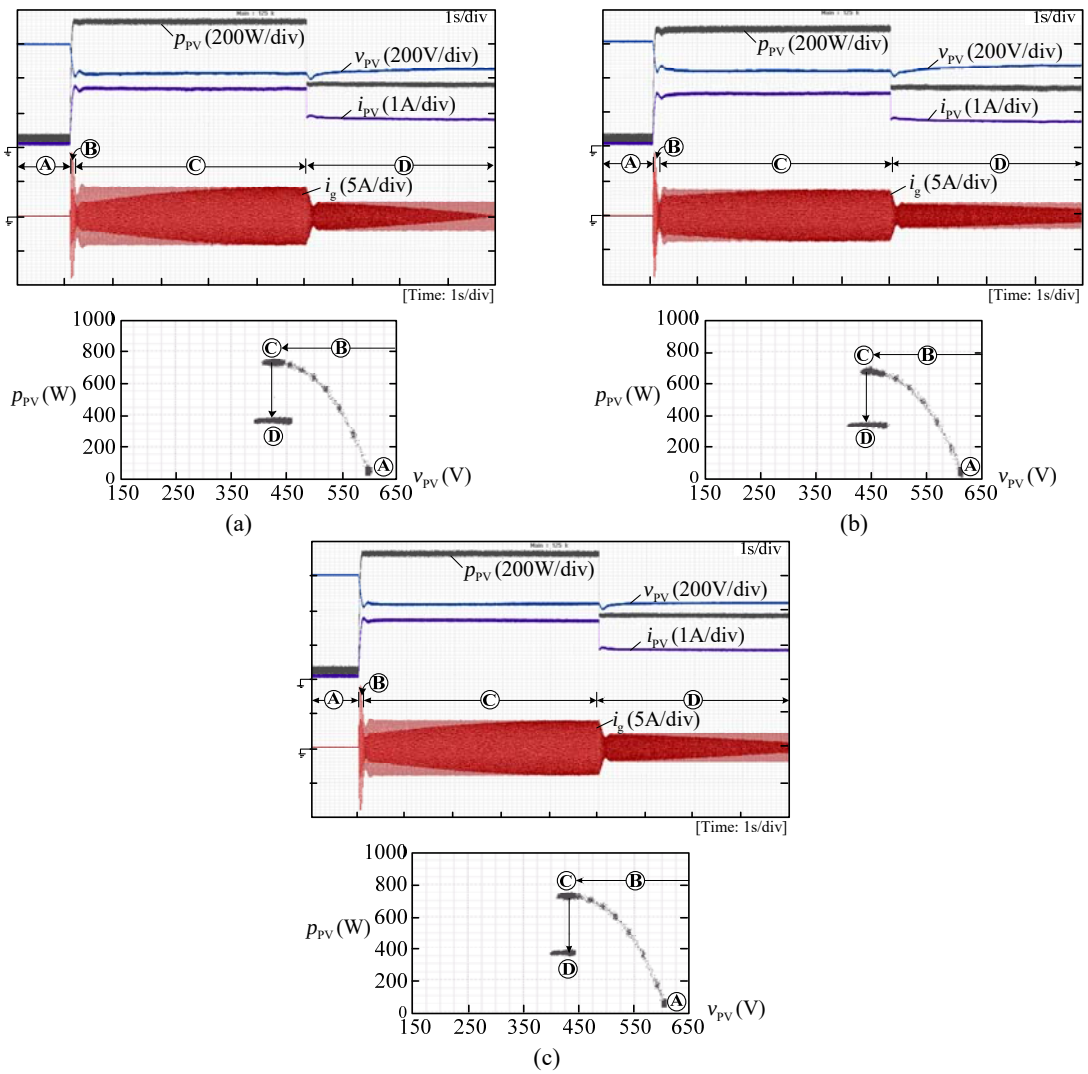

Fig. 12. Experimental results of system response since starting operation. (a) Modified RCC MPPT method. (b) Conventional RCC MPPT. (c) P&O MPPT.

period A in the corresponding *P–V* curve. When the proposed MPPT algorithm is started during period B, the proposed MPPT algorithm attempts to track the MPP from this period to period C with the increments of the PV power and current, but the PV voltage is decreased. Hereby, the instantaneous injection of the grid current via the H-bridge VSI is then conducted. Until the PV power reaches the MPP at 731 W in period C, the PV current and voltage are approximately 1.68 A and 435 V, which is theoretically analyzed to be approximately 79% of the open-circuit voltage. As expected, it can supply a 682 W power to the interfacing utility grid. Then, the 50% shading condition is also examined by disconnecting a PV string, as shown from periods C to D, where the response is similar to the stepped-down response from periods C to D of the prior case study discussed in Fig. 9. The comparison between the proposed MPPT method and the two results of the conventional methods shows that the responses of the system in these three MPPT methods are the same. That is, the performance of the proposed modified RCC MPPT method is able to track the MPP, whether it is the starting, dynamic changing or steady-state or any possible shading condition, where the performance is equivalent to that of the existing and well-known RCC MPPT and P&O MPPT methods. Furthermore, during the step dynamic changes for start and shading operations, the desirable MPPTs are immediately satisfactory for all the PV voltage v_{PV}, and the PV power p_{PV}, PV current i_{PV}, and grid current i_g, in accordance with the proposed method (see Fig. 12(a)), thereby conforming with those of the existing methods in Figs. 12(b) and 12(c).

V. Conclusions

In this study, a modified RCC MPPT algorithm using the simple arithmetic mean function has been proposed and validated for the single-stage single-phase VSI grid-connected PV system. This algorithm does not need filters to generate the PV power and PV voltage ripples and the average value of the ripple product. In addition, an AC component filter is not required in the part of a PI voltage controller. A high-accuracy and high-precision MPPT has been achieved during steady-state and dynamic shading operating conditions. The simulation and experimental results confirm the performance of the proposed control algorithm for the single-stage single-phase VSI grid-connected PV system.

Acknowledgment

This study was supported in part by the Thailand Research Fund under Grant RSA5880006 and in part by the Chiang Mai University Mid-career Research Fellowship Program.

References

[1] S. B. Kjaer, J. K. Pedersen, and F. Blaabjerg, "A review of single-phase grid-connected inverters for photovoltaic modules," *IEEE Trans. Ind. Appl.,* Vol. 41, No. 5, pp. 1292-1306, Sep./Oct. 2005.

[2] J. Kim and S. Sul, "Transformerless inverter for single-phase photovoltaic systems," *IEEE Trans. Power Electron.*, Vol. 22, No. 2, pp. 693-697, Mar. 2007.

[3] Y. Yang, F. Blaabjerg, and H. Wang, "Low-voltage ride-through of single-phase transformerless photovoltaic inverters," *IEEE Trans. Ind. Appl.,* Vol. 50, No. 3, pp. 1942-1952, May/Jun. 2014.

[4] W. Li, Y. Gu, H. Luo, W. Cui, X. He, and C. Hia, "Topology review and derivation methology of single-phase transformerless photovoltaic inverters for leakage current suppression," *IEEE Trans. Ind. Electron.,* Vol. 62, No. 7, pp. 4537-4551, Jul. 2015.

[5] E. Villanueva, P. Correa, J. Rodríguez and M. Pacas, "Control of a single-phase cascaded H-bridge multilevel inverter for grid-connected photovoltaic systems," *IEEE Trans. Ind. Electron.,* Vol. 56, No. 11, pp. 4399-4406, Nov. 2009.

[6] R. A. Mastromauro, M. Liserre, and A. Dell, "Control issues in single-stage photovoltaic systems: MPPT current and voltage control," *IEEE Trans. Ind. Infomat.*, Vol. 8, No. 2, pp. 241-254, May 2012.

[7] M. Ebrahimi, S. A. Khajehoddin, and M. K. Ghartemani, "Fast and robust single-phase DQ current controller for smart inverter applications," *IEEE Trans. Power Electron.*, Vol. 31, No. 5, pp. 3968-3976, May. 2006.

[8] M. A. G. de Brito, L. Galotto, Jr., L. P. Sampaio, G. de A. e Melo, and C. A. Canesin, "Evaluation of the main MPPT techniques for photovoltaic applications," *IEEE Trans. Ind. Electron.,* Vol. 60, No. 3, pp. 1156-1167, Mar. 2013.

[9] D. Sera, R. Teodorescu, J. Hantschel, and M. Knoll, "Optimized maximum power point tracking for fast-changing environmental conditions," *IEEE Trans. Ind. Electron.,* Vol. 55, No. 7, pp. 2629 - 2637, July. 2008.

[10] R. Kadri, J.-P. Gaubert, and G. Champenois, "An improved maximum power point tracking for photovoltaic grid-connected inverter based on voltage-oriented control," *IEEE Trans. Ind. Electron.,* Vol. 58, No. 1, pp. 66-75, Jan. 2011.

[11] N. Femia, G. Petrone, G. Spagnuolo, and M. Vitelli, "A technique for improving P&O MPPT performances of double-stage grid-connected photovoltaic systems," *IEEE Trans. Ind. Electron.,* Vol. 56, No. 11, pp. 4473-4482, Nov. 2009.

[12] D. G. Montoya, C. A. R.-Paja and R. Giral, "Improved design of sliding-mode controllers based on the requirement of MPPT techniques," *IEEE Trans. Power Electron.*, Vol. 31, No. 1, pp. 234-247, Jan. 2016.

[13] S. B. Kjaer, "Evaluation of "Hill climbing" and the "Incremental conductance" maximum power point trackers for photovoltaic power systems," *IEEE Trans. Energy Convers.*, Vol. 27, No. 4, pp. 922-929, Dec. 2012.

[14] A. Safari and S. Mekhilef, "Simulation and hardware implementation of incremental conductance MPPT with direct control method using cuk converter," *IEEE Trans. Ind. Electron.,* Vol. 58, No. 4, pp. 1154-1161, Apr. 2011.

[15] T. Esram, J. W. Kimball, P. T. Krein, P. L. Chapman, and P. Midya, "Dynamic maximum power point tracking of photovoltaic arrays using ripple correlation control," *IEEE Trans. Power Electron.*, Vol. 21, No. 5, pp. 1282-1291,

Sep. 2006.
[16] C. Barth and R. C. N. P.-Podgurski, "Dithering digital ripple correlation control for photovoltaic maximum power point tracking," *IEEE Trans. Power Electron.*, Vol. 30, No. 8, pp. 4548-4559, Aug. 2015.
[17] S. L. Brunton, C. W. Rowley, S. R. Kulka, and C. Clarkson, "Maximum power point tracking for photovoltaic optimization using ripple-based extremum seeking control," *IEEE Trans. Power Electron.*, Vol. 25, No. 10, pp. 2531-2540, Oct. 2010.
[18] A. M. Bazzi and P. T. Krein, "Ripple correlation control: an extremum seeking control perspective for real-time optimization," *IEEE Trans. Power Electron.*, Vol. 29, No. 02, pp. 988-995, Feb. 2014.
[19] R. Khanna, Q. Zhang, W. E. Stanchina, G. F. Reed, and Z.-H. Mao, "Maximum power point tracking using model reference adaptive control," *IEEE Trans. Power Electron.*, Vol. 29, No. 3, pp. 1490-1499, Mar. 2014.
[20] D. Casadei, G. Grandi, and C. Rossi, "Single-phase single-stage photovoltaic generation system based on a ripple correlation control maximum power point tracking," *IEEE Trans. Energy convers.*, Vol. 21, No. 2, pp. 562-568, Jun. 2006.
[21] S. Golestan, M. Ramezani, J. M. Guerrero, F. D. Freijedo, and M. Monfared, "Moving average filter based phase-locked loops: performance analysis and design guidelines," *IEEE Trans. Power Electron.*, Vol. 29, No. 6, pp. 2750-2763, Jun. 2014.
[22] C. Boonmee and Y. Kumsuwan, "Modified maximum power point tracking based-on ripple correlation control application for single-phase VSI grid-connected PV systems," in *Proc. IEEE Conf., ECTI-CON 2013*, pp. 1-6.
[23] C. Boonmee and Y. Kumsuwan, "Control of single-phase cascaded H-bridge multilevel inverter with modified MPPT for grid-connected photovoltaic systems," in *Proc. IEEE Conf., IECON 2013*, pp. 566-571, 2013.

Chaiyant Boonmee received his B. Eng and M. Eng degrees in electrical engineering from Rajamangala Institute of Technology Thewes and Rajamangala University of Technology Thanyaburi, Thailand, in 1991 and 2010, respectively. He is currently working on his Ph.D. degree in electrical engineering at Chiang Mai University. His research interests include power electronic application and multilevel cascaded inverters.

Yuttana Kumsuwan (M'12) received his Ph.D. degree in electrical engineering from Chiang Mai University (CMU), Chiang Mai, Thailand, in 2007. He was a visiting professor at Texas A&M University, College Station, from October 2007 to May 2008, and at Ryerson University, Toronto, ON, Canada, from March to May 2010. Since 2014, he has been an Associate Professor at the Department of Electrical Engineering, Faculty of Engineering, CMU. His research interests include power converters, PWM techniques, multilevel converters, energy conversion systems, and electric drives.